Development and Verification of Ferroptosis-Related Gene Signature for Predicting the Prognosis and Immune Microenvironment in Gastric Cancer

Siyuan Song
Affiliated Hospital of Nanjing University of Chinese Medicine
Peng Shu (shupengnjucm@163.com)
Affiliated Hospital of Nanjing University of Chinese Medicine

Research Article

Keywords:

Posted Date: February 7th, 2022

DOI: https://doi.org/10.21203/rs.3.rs-1235765/v1

Abstract

Objective:

The study is to explore the role of ferroptosis-related genes (FRGs) in the occurrence and development of gastric cancer (GC), and to construct a new prognosis signature to predict the prognosis and immune microenvironment in GC.

Method:

We downloaded RNA sequencing data and related clinical information of GC from the Cancer Genome Atlas (TCGA-STAD) database as a training cohort. Microarray GSE84426 and GSE84437 were downloaded from Gene expression synthesis (GEO) database as validation cohorts. FRGs were come from FerDb. Prognostic genes associated with ferroptosis were identified in the training cohort using univariate Cox analysis and venn diagram, and two different molecular subtypes were identified by consistent clustering. Kaplan-Meier survival curve verified the prognostic value. ESTIMATE, CIBERSORT, McpCounter and TIMER algorithm were used to analyze the infiltration of immune cells in each sample. LASSO algorithm and multiple Cox regression analysis were used to construct a prognostic risk signature and verified it. Finally, gene set enrichment analysis (GSEA) revealed several important ways to participate in GC.

Result: We obtained 16 prognostic genes for GC associated with ferroptosis, and divided GC patients into two subgroups by consistent clustering. Cluster C2 showed obvious median survival advantage, while Cluster C1 showed poor prognosis. Compared with Cluster C2, GC patients in Cluster C1 have significantly higher ESTIMATE score, higher immune cell infiltration and higher matrix score. MCPCounter, TIMER and CIBERSORT algorithms also showed that Cluster C1 had more immune cell infiltration, suggesting that the tumor immune microenvironment (TIME) of GC patients in high-risk group Cluster C1 accorded with immune exclusion subtype. Based on LASSO analysis, a risk signature was established, and it was found that TUBE1, NFE2L2 and ACSL4 genes were protective factors, while ZFP36, NOX5 and MIR9-3 genes were risk factors. Through the verification of GEO cohort, the risk signature of FRGs had a great potential to predict the prognosis of GC patients, and it was a strong correlation between the prognosis signature and GC immunity. The nomogram combined with risk signature and clinical features can accurately predict the prognosis of GC patients. GSEA analysis showed that compared with Cluster C2, Cluster C1 had lower expression in lipid metabolism and glutathione metabolism, which may be related to poor prognosis of GC patients.

Conclusion: We constructed a new prognostic signature based on ferroptosis-related prognostic genes to predict the prognosis and TIME in GC, and the development of this signature had provided a new clue for determining the relationship between ferroptosis and immunity, which can be used to accurately predict the prognosis of GC patients and provide new strategies for immunotherapy of GC patients.

1. Introduction

Gastric cancer (GC) is the fourth leading cause of cancer-related death [1], GC has the highest incidence among digestive tract malignant tumors in China[2].Because the early stage of GC is usually asymptomatic, it is mostly late when it is discovered, resulting in a 5-year overall survival rate (OS) of less than 40%[3].Therefore, exploring new and more effective treatment methods has become a problem to be solved.

The occurrence and development of tumors are closely related to cell death. Ferroptosis is a form of non-apoptotic cell death found in recent years[4].Triggered by lipid reactive oxygen species (ROS) [5] Ferroptosis is related to the occurrence of many kinds of tumors, including lung cancer[6], breast cancer[7], colorectal cancer[8],and GC [9]. In recent years, many ferroptosis genes including GPX4, SLC7A11 and NRF2 have been found to be promising targets for inducing tumor cell death. Therefore, targeting ferroptosis may be a new strategy for cancer treatment.

Tumor immunotherapy, as a new treatment method based on human immune system, plays an anti-tumor role by immune regulation. The use of checkpoint inhibitors has been proved to be of great significance in improving the objective remission rate of tumors and prolonging the survival time of patients [10, 11]. Tumor infiltrating immune cells (TIIC) are related to many kinds of tumor prognosis and immunotherapy response [12–14]. For example, M2 macrophages are enriched in bladder cancer tissue, which can be used as a potential immunotherapy target for bladder cancer [15]. Many kinds of tumor immunotherapy related to natural killer cells (NK) have also entered the clinical trial stage [16]. It has been proved that TIME is closely related to the pathogenesis of GC [17]. Therefore, mining immune cell-related targets is an effective way to optimize tumor immunotherapy[18] .

In this study, we comprehensively analyzed the genes related to ferroptosis to explore the influence of ferroptosis on the survival of patients with GC. In addition, we constructed and verified a risk signature of FRGs to evaluate the prognostic value in GC. The functional enrichment analysis was carried out to explore the potential mechanism and provide a new strategy for targeted and individualized treatment of GC. The protocol of our study procedures is shown in Figure 1.

2. Method

2.1 Data acquisition and analysis

The FPKAPLAN-MEIER ANALYSIS gene expression profile of GC (TCGA-STAD) was obtained from TCGA database (https ://portal.gdc.cancer.gov/). As a training cohort, we obtained 443 clinical samples, including 375 samples of cancer tissues and 68 samples of adjacent tissues. We extracted the mapping information of GeneSymbol and ENSG_ID, mapped the ENSG_ID to GeneSymbol, and when there were multiple matches, took the median, and finally obtained the transformed expression spectrum. Finally, the data was further standardized by log2(X+1) transformation. The microarray data GSE84426 and GSE84437 were downloaded from GEO database (http://www.ncbi.nlm.http://nih.gov/geo/) through GPL6947 application platform. As validation cohorts, we obtained 509 GC tissue samples. Clinical

information of the above patient is shown in Table 1. 259 genes related to ferroptosis were collected from FerrDB (http://www.zhounan.org/ferrdb/) database[19], including driver, suppressor, and marker.

Table 1
Clinical characteristic of the GC patient used in this study

	TCGA	GEO
No. of patients	443	509
Age (%)		
≤65	246(55.5)	325(63.8)
65	197(44.5)	184(36.2)
Gender (%)		
Female	158(35.6)	159(31.2)
Male	285(64.4)	350(68.8)
Grade (%)		
G1	12(2.7)	NA
G2	159(35.9)	NA
G3	263(59.4)	NA
GX	9(2)	NA
Stage (%)		
I	59(13.3)	NA
II	97(21.9)	NA
III	183(41.3)	NA
IV	44(23.5)	NA
Survival status		
OS day(median)	413	2070
Ending (%)		
Survival	270(60.9)	265(52.1)
Death	173(39.1)	244(47.9)

2.2 Molecular subtype identification

The genes related to the prognosis of GC were screened out by univariate Cox regression analysis. Venn diagram was used to intersect the prognosis-related genes of GC with ferroptosis genes to obtain ferroptosis-related prognosis genes. The R package "ConsensusClusterPlus" was used to screen the prognostic genes related to ferroptosis.

2.3 Immune analysis

Immunological analysis was used to explore the immune differences between the two subgroups. Estimate (estimation of violent and immune cells in malignant tumor organization using expression) algorithm is used to evaluate the proportion of immune-matrix components in TIME, include Stromal Score (reflecting the presence of matrix), Immune Score (reflecting the level of immune cell infiltration) and ESTIMAT Score (comprehensive score of immunity and matrix) [20]. The higher the corresponding score, the larger the proportion of corresponding components in TIME. Use MCP Counter and TIMER database [21] to predict the infiltration level of immune cells in GC. CIBERSORT algorithm was used to estimate the data of tumor infiltrating immune cells[22]. The activity of immune-related pathways in each GC patient was quantified by "GSEA" R package [23].

2.4 Construction of risk scoring signature based on ferroptosis related prognostic genes

The " glmnet " R package was used for LASSO analysis to further select key prognostic markers, and the minimum lambda was defined as the optimal value. According to the risk score of the established prognosis signature, GC patients were divided into high and low risk groups. Kaplan-Meier survival curve and time-dependent ROC curve were used to analyze and compare the survival situation between the two groups. Immunohistochemical staining of key prognostic genes of ferroptosis was examined by human protein atlas (HPA) (https://www.proteinatlas.org/about/download). Maftools was used to calculate the mutation of key prognostic genes of ferroptosis in training cohort, and ggplot2 package [24] was used to draw the mutation distribution map.

2.5 Validation of prognostic risk signature

COX regression and subgroup analysis were used to evaluate the independence of the prognosis signature and the clinical characteristics (including gender, age and stage) of patients, and the survival differences between high and low risk groups were evaluated according to gender and age. The GEO validation cohort was used to verify the prediction accuracy of the established prognosis signature. Combining the prognosis signature and clinical features, nomogram was constructed to predict the 1,3 and 5-year survival rate of GC patients.

2.6 DEGs identification and Functional Enrichment Analysis

According to the two molecular subtypes, the differentially expressed genes (DEGs) in the training cohort were identified by "limma" R package, and the false discovery rate (FDR) was less than 0.05, and the difference multiple was 1.5 times as the screening standard. GSEA enrichment analysis was carried out according to DEGs. Metascape software was used to construct PPI network of DEGs [25].

2.7 Statistical analysis

All statistical analysis in this paper was carried out by R software. All values of statistical data were based on two groups of statistical tests. P < 0.05 was considered to be statistically significant.

3. Results

3.1 Identification of molecular subtypes based on ferroptosis

Through COX univariate analysis, we obtained 2,381 GC prognosis-related genes, and 16 GC prognostic genes associated with ferroptosis were obtained by intersecting 2,381 GC prognosis-related genes with 259 ferroptosis genes (Figure 2A). GC were divided into two subgroups using consistent clustering (Figure 2B-E), Cluster C1 included 210 patients, while Cluster C2 included 197 patients. The two subgroups were visualized by heat map (Figure 2F). Kaplan-Meier survival curves of two different subgroups showed that Cluster C2 showed significant median survival advantage, while Cluster C1 showed poor prognosis (Figure 2G).

3.2 Immune microenvironment of two different molecular subtypes

The ESTIMATE algorithm showed significantly higher ESTIMATE scores (P < 0.0001), higher immunocyte infiltration (P < 0.01), and higher matrix score (P < 0.0001) for GC patients in Cluster C1 compared with Cluster C2 (Figure 3A), suggesting that the tumor immune microenvironment of GC patients in Cluster C1 group in the high-risk group conformed to the immune exclusion subtype. The MCPCounter algorithm showed that the expression levels of B-lineage (P < 0.00), Myoid-Dendritic-cells (P < 0.0001), Neutrophils (P < 0.01), Endothelial-cells (P < 0.0001) and Fibroblasts (P < 0.0001) in Cluster C1 were significantly higher than those in Cluster C2 (Figure 3B). The TIMER algorithm showed that fibrolasts (p = 7.80e-12), CD4+T cells (p = 0.0009), and B cells (p = 0.0023) were significantly higher in Cluster C1 than in Cluster C2 (Figure 3C-D). The CIBERSORT algorithm indicated Macrophases-M0 (p = 0.0000052), CD4 Memory Activated-T cells (p = 0.00024), Macrophases-M1 (p = 0.001), Nave-B-cells (p = 0.001), NK cells (P = 0.02) were significantly higher in Cluster C1 than in Cluster C2 (Figure 3E-F), suggesting a relatively low immune state in Cluster C2. These results indicated a significant difference in the immune microenvironment of the two molecular subtypes.

3.3 Construction of risk signature based on prognosis genes related to ferroptosis

We signatureed the risk based on LASSO analysis, and we set the lambda value to be 0.029411686746793, Built signature RiskScore = [0.17987688835102 * ZFP36]-[0.2111220517453 * TUBE1]-[0.1164248611519 * SLC1A4]+[1.958393356095 * NOX5]+[0.480740705518259*NOX4]-

[0.39552084635819*NFE2L2]+[2.63582963497227*MIR9]-[0.0833648850166638*GCH1]+[0.702888544996765*GABARAPL2]-[0.117744902736126*CHAC1] +[0.010366289402305 * CAPG]-[0.25896183370357 * ACSL4]-[0.033599913666074 * ACO1], 13 genes were finally obtained, and three of them were risk genes with the risk ratio greater than 1. Then we analyzed the relationship between different risk scores and survival state of patients. We observed that with the increase of risk score, the survival rate of patients decreased significantly. TUBE1, NFE2L2, and ACSL4 genes were protective factors, because the expression showed a downward trend with the increase of risk score. ZFP36, NOX5, and MIR9-3 genes were risk factors, because the expression showed an upward trend with the increase of risk score (Figure 4A). The risk signature established divided GC patients into high-risk group and low-risk group (Figure 4B). Kaplan-Meier analysis showed that all the constructed prognostic genes were independent prognostic markers for GC patients (Figure 4C). Based on the information such as the survival state and survival time of the patients, we drew the forest map for multivariate survival analysis of prognostic genes (Figure 4D). The ROC curve (Figure 4E) showed the reliability and stability of the risk signature constructed. ROC analysis showed that the risk signature constructed exhibited accurate prediction ability within 5 years, with AUC of 0.69, 0.80 and 0.81 for 1, 3 and 5 years, respectively. Finally, the TIME of the two groups was evaluated using the ESTIMATE algorithm, and the results showed that the high-risk group had a higher ESTIMATE score (P =1.2e-4), higher immune cell infiltration (P= 4.8e-7), and higher matrix score (P = 5.1e-7) (Figure 4F). The TIMER database was used to predict the relationship between the key prognostic genes for ferroptosis and the infiltration level of immune cells, and it was found that the key prognostic genes for ferroptosis were closely related to the infiltration of macrophages, B cells, T cells, dendritic cells, and neutrophils (Figure 4G). These results indicated that the risk signature constructed had a strong potential for prognosis prediction of GC patients, and it was a strong correlation between this prognosis signature and GC immunity. The HPA database examined the immunohistochemical staining of 13 critical prognostic genes for ferroptosis (Figure 5) and found that the protein expressions of ZFP36, TUBE1, NFE2L2, GCH1, GABARAPL2, CHAC1, CAPG, ACSL4, ACO1, and SLC1A4 in GC and normal tissues were significantly different, and there was no protein expression of NOX5, MIR9-3, and NOX4 in HPA. In addition, we observed mutations in the key prognostic genes for ferroptosis in the training cohort and found that TUBE1 was a dominant gene and therefore better targeted (Figure 6).

The expression of ZFP36, TUBE1, NFE2L2, GCH1, GABARAPL2, CHAC1, CAPG, ACSL4, and ACO1 in the HPA.

3.4 Validation of prognostic risk signature

We assessed the differences in risk scores among the subgroups by age (Figure 7A), gender (Figure 7B), T (Figure 7C), N (Figure 7D), Stage (Figure 7E), and Grade (Figure 7F) and found no significant differences between the subgroups, indicating that the risk scores were not correlated with the clinical characteristics of the patient. The Kaplan-Meier curves between high and low-risk groups were drawn according to the age (Figure 7G-H) and gender (Figure 7I-J). It was found that the prognosis of patients in the high-risk group was poor, while the prognosis of patients in the low- risk group was good. This

indicated that the prognosis signature we constructed can be used to independently predict the prognosis of GC patients. To verify the stability of the prognostic signature developed in the training cohort, we calculated the risk score for each patient in the validation cohort using the same formula as in the build training cohort. Patients in the validation cohort were grouped into high-risk (n=216) and low-risk (n=293) subgroups (Figure 8A) and ROC analysis revealed AUC values of 0.63, 0.65, and 0.69 at 1, 3, and 5 years, respectively (Figure 8B). The KAPLAN-MEIER ANALYSIS curve showed that the low- risk group had a better prognosis than the high-risk group (Figure 8C). In addition, the ESTIMATE algorithm was performed on high-risk and low-risk groups in the validation cohort, and the results showed significant differences between the two subgroups in matrix score, and tumor purity (Figure 8D-G), and the high-risk group had higher matrix score, higher ESTIMATE score, and lower tumor purity. The 1,3 and 5-year survival rates observed with the Nomogram were well matched to the actual survival rates, demonstrating that the Nomogram can well predict the prognosis of GC patients (Figure 8H-I).

Differences in risk scores among(A)Age, (B)Gender, (C)T, (D)N, (E) Stage, and (F)Grade. Survival curve of GC patients regrouped according to age (G-H), and gender (I-J). *p < 0.05; **p < 0.01; ***p < 0.001.

3.5 DEGs identification and Functional Enrichment Analysis

A total of 570 DEGs were detected compared to Cluster C2, of which 465 genes were up-regulated and 105 genes were down-regulated in Cluster C1 (Figure 9A-B). GO enrichment analysis showed that the BP of DEGs mainly included cell migration, immune globulin, human immune response mediated by circulating immune globulin. CC was mainly enriched in the extracellular matrix. MF mainly included immunoglobulin receptor binding, fibronectin binding, and growth factor binding (Figure 9C-G). The KEGG enrichment analysis showed that DEGs was mainly enriched in the Cell cycle, p53 signaling pathway, IL-17 signaling pathway, MAPK signaling pathway, and PI3K-Akt signaling pathway (Figure 9H-I). To further explore the relationship between enrichment pathways and prognosis of GC patients, we performed GSEA analysis, and the results showed that compared with Cluster C2, Cluster C1 showed lower expression in lipid metabolism and glutathione metabolism, which might be related to the poor prognosis of GC patients (Figure 9J).

4. Discussion

In recent years, various prognostic signatures have been proposed to predict the prognosis and immune infiltration of malignant tumors[26]. Including predicting the immune infiltration state and prognosis of malignant tumors by screening immune-related genes or FRGs, and few studies have used a method of combining the FRGs with the immune-related genes to predict the immune infiltration state and prognosis of tumors. Therefore, in this study, an ferroptosis-related prognosis signature was constructed by combining ferroptosis with immunity to better predict the prognosis and immune response of GC patients.

Firstly, we obtained 16 GC prognostic genes related to ferroptosis, and divided GC patients into two subgroups by consistent clustering. Cluster C2 showed a significant median survival advantage, while Cluster C1 showed a poor prognosis. Compared with Cluster C1, GC patients in Cluster C1 had

significantly higher ESTIMATE score, higher immunocyte infiltration and higher matrix score. MCPCounter, TIMER and CIBERSORT algorithms also indicated that Cluster C1 had more immunocyte infiltration, which indicated that high-risk groups have higher levels of immunocyte infiltration and interstitial components in the tumor microenvironment. TME is generally divided into three categories: immune inflammation, immune rejection and immune desert [27]. In this study, based on the high-risk group's manifestations of high immune cell infiltration abundance and large proportion of interstitial components but with poor prognosis, it was speculated that TME in Cluster C1 of the high-risk group met the immune exclusion subtype. Although the TME of the patients in the Cluster C1 group had a large number of immunocyte infiltrates, they were not effective at penetrating the tumor parenchyma to eliminate tumor cells. Therefore, the prognosis of high-risk group was often poor. Subsequently, a risk signature was constructed based on LASSO analysis, and 13 genes were finally obtained, which showed that TUBE1, NFE2L2, ACSL4 genes were protective factors, while ZFP36, NOX5, and MIR9-3 genes were risk factors. Kaplan-Meier analysis showed that all the constructed prognostic genes were independent prognostic markers for GC patients.The ROC curve showed the reliability and stability of the risk signature constructed. The ESTIMATE algorithm was used to evaluate the TIME between the high-risk group and the low-risk group. The results showed that the high-risk group had higher ESTIMATE score, higher immune cell infiltration and higher matrix score, which were the same as the results of the above study, suggesting that TME in the high-risk group met the immunologic exclusion subtype. The TIMER database showed that the key prognostic genes for ferroptosis were closely related to the infiltration of macrophages, B cells, T cells, dendritic cells, and neutrophils. The HPA database examined the immunohistochemical staining of 13 critical prognostic genes for ferroptosis and found that the protein expressions of ZFP36, TUBE1, NFE2L2, GCH1, GABARAPL2, CHAC1, CAPG, ACSL4, ACO1, and SLC1A4 in GC and normal tissues were significantly different, and there was no expression of NOX5, MIR9-3, and NOX4 proteins in the HPA. A study had shown that autophagy promotes ferroptosis by degrading anti-iron death factors [28], and ZFP36 was a key protein for autophagy and considered to be related to ferroptosis [29]. NFE2L2, a known transcription factor involved in the encoding of GC development, is overexpressed as a prognostic marker of GC [30]. OS rate in GC patients with NRF2 positive expression was significantly reduced[31]. The experiment conducted by Wei [32] proved that GCH1 induced immunosuppression through a 5-HTP-AHR-ID01-dependent mechanism, and that the combination of metabolic intervention and immunotherapy of this pathway might be a promising strategy for the treatment of triple-negative breast cancer (TNBC), and the GCH1 inhibitor could be used as an analgesic [33]. Members of the GABARAP family (GABARAP, GABARAPL1/GEC1 and GABARAPL2/GATE-16) are one of the subfamilies of the ATG8 protein family, which are related to the receptor and autophagy pathway[34]. The high-expression of GABARAP is related to the good prognosis of tumors[35].CHAC1 is an enzyme related to the activity of γ-glutamyl cyclotransferase that can degrade intracellular GSH and promote ferroptosis of tumor cells[36], which has been proved to be related to glioma [37]and breast cancer [38]. CAPG is particularly abundant in macrophage expression [39], and CAPG had been proved to be related to tumor cell invasion and tumorigenic [40]. SLC1A4 is one of the members of solute carrier family 1(SLC1), and SLC1A4 is one of the important roles of amino acid transporter [41]. SLC1A4 is highly expressed in pancreatic ductal adenocarcinoma and liver cancer cells, and some studies have suggested

that SLC1A4 may promote the process of ferroptosis[42]. ACSL4, a long-chain fatty acyl coenzyme, is closely related to the proliferation and migration of tumor cells[43]. ACSL4 had been shown to be overexpressed in breast cancer [44], GC[45], and liver cancer[46]. ACO1(Cytoplasmic aconitic acid hydratase) is a protein that participates in cytoplasmic and mitochondrial metabolism and, when down-regulated, leads to cell death [47]. NOX is a family of encoded oxidases, NOX4 is a catalytic subunit of nicotinamide adenine dinucleotide phosphate (NADPH) oxidase complex, and NOX5 mainly encodes calcium-dependent NADPH oxidase, produces superoxide, and acts as a calcium-dependent proton channel. The ROS produced by NOX4 is involved in a variety of biological functions, including signal transduction, cell differentiation and tumor cell growth [48, 49], and NOX4 plays an important role in the process of ferroptosis [50]. Inhibition of NOX4 can significantly block ferroptosis[51]. MiRNA plays an important role in tumors. MiR-9 is overexpressed in lung cancer tissues[52], and MiR-9 acts as a biomarker for poor prognosis in lung cancer and thyroid papillary carcinoma[53]. There is no report about the relationship between TUBE1 and tumor in the literature. These results indicated that the risk signature constructed had a strong potential for prognosis prediction of GC patients, and there was a strong correlation between this prognosis signature and GC immunity.

We verified the accuracy of the constructed prognostic signature by verifying the cohort, and the results showed that this prognostic signature had a strong potential for prognosis prediction of GC patients, and there was a strong correlation between this prognostic signature and GC immunity. Nomograms that combine risk signatures with clinical features can accurately predict the prognosis of patients with GC.

Finally, KEGG enrichment analysis showed that DEGs was mainly enriched in the Cell cycle, p53 signaling pathway, IL-17 signaling pathway, MAPK signaling pathway, and PI3K-Akt signaling pathway. p53 is a tumor suppressor gene, and p53 mutations have been reported in many cancers[54]. When p53 mutations occur, cells proliferate abnormally and transform into cancer cells. GC patients with p53 mutation have worse prognosis than those without mutation [55]. More and more evidences support the pathogenic role of IL-17 in cancer formation, including colon cancer [56] and lung cancer [57]. Wu [58]found that IL-17 could promote tumor angiogenesis by mediating the up-regulation of VEGF in GC through STAT3 pathway. It has been confirmed that MAPK and PI3K-Akt pathways are involved in many processes of the occurrence and development of GC[59–61]. The results of GSEA analysis showed that compared with Cluster C2, Cluster C1 had low expression in lipid metabolism and glutathione metabolism, which were important metabolic pathways in the occurrence of ferroptosis, which might be related to the poor prognosis of GC.

The above results indicated that the expression of prognosis genes related to ferroptosis was related to the immune microenvironment of GC patients. It can be used to accurately predict the prognosis of GC patients and provide a new strategy for immunotherapy of GC patients.

However, this study has certain limitations. Our signature was constructed and validated based on retrospective data, without relevant experimental verification.

5. Conclusion

The results of this study showed that the expression of prognosis genes related to ferroptosis was related to the immune microenvironment of GC patients. Based on the prognosis genes related to ferroptosis, we constructed a new prognosis signature to predict the prognosis and immune status of GC. The development of this signature has provided new clues for determining the relationship between ferroptosis and immunity, which can be used to accurately predict the prognosis of GC patients and provide new strategies for the immunotherapy of GC patients.

Abbreviations

TCGA: The Cancer Genome Atlas

GEO: Gene Expression Omnibus

GC: Gastric Cancer

FRGs: Ferroptosis-related genes

GSEA: Gene set enrichment analysis

TIME: tumor immune microenvironment

TIIC: Tumor infiltrating immune cells

HPA: Human protein atlas

DEGs: Differentially expressed genes

GO: Gene Ontology

BP: Biological process

CC: Cellular component

MF: Molecular function

FDR: Error Detection Rate

KEGG: Kyoto Encyclopedia of Genes and Genomes

PPI: Protein-protein interaction

Overall Survival: OS

Declarations

Statement

All methods were carried out in accordance with relevant guidelines and regulations.

Data Availability

The data used to support the findings of this study are included within the article, and we uploaded the raw data in the system.

The datasets generated and/or analysed during the current study are available in the TCGA (https ://portal.gdc.cancer.gov/)GEO(http://www.ncbi.nlm.http://nih.gov/geo/)

FerrDB (http://www.zhounan.org/ferrdb/)

and (HPA) (https://www.proteinatlas.org/about/download)database repository.

Conflicts of Interest

The authors declare that there are no conflicts of interest.

Authors' Contributions

Peng Shu designed the research. Siyuan Song analyzed the data and wrote the paper, Jiayu Zhou, Ye Li, Jiatong Liu, Jinzhan Li, Xingxing Zhang, Wanru Zhang and Hongyan Wu selected the materials. All authors read and approved the submitted version.

Acknowledgments

This work was funded by the National Natural Science Foundation of China (nos. 81673918). Pilot GC project of clinical collaboration of traditional Chinese medicine and Western medicine on major difficult diseases in the state administration of traditional chinese medicine; 2019"Construction Project of Evidence-based Capacity for Traditional Chinese Medicine"(2019XZZX-ZL003) in state administration of traditional chinese medicine; Open Program of the Third Phase of the Program of Traditional Chinese Medicine (TCM) Advantageous Subjects (ZYX03KF020); Science and Technology Project of Jiangsu Provincial Administration of Traditional Chinese Medicine (ZD201803).

References

1. Ferlay J, Colombet M, Soerjomataram I, Parkin DM, Pineros M, Znaor A, Bray F: **Cancer statistics for the year 2020: An overview**. *Int J Cancer* 2021.
2. Hironaka S: **Anti-angiogenic therapies for GC**. *Asia Pac J Clin Oncol* 2019, **15**(4):208–217.
3. Zheng S, Zhang Z, Ding N, Sun J, Lin Y, Chen J, Zhong J, Shao L, Lin Z, Xue M: **Identification of the angiogenesis related genes for predicting prognosis of patients with GC**. *BMC Gastroenterol* 2021, **21**(1):146.

4. Dixon SJ, Lemberg KAPLAN-MEIER ANALYSIS, Lamprecht MR, Skouta R, Zaitsev EM, Gleason CE, Patel DN, Bauer AJ, Cantley AM, Yang WS *et al*: **Ferroptosis: an iron-dependent form of nonapoptotic cell death**. *Cell* 2012, **149**(5):1060–1072.
5. Zhao Y, Hu X, Liu Y, Dong S, Wen Z, He W, Zhang S, Huang Q, Shi M: **ROS signaling under metabolic stress: cross-talk between AMPK and AKT pathway**. *Mol Cancer* 2017, **16**(1):79.
6. Lai Y, Zhang Z, Li J, Li W, Huang Z, Zhang C, Li X, Zhao J: **STYK1/NOK correlates with ferroptosis in non-small cell lung carcinoma**. *Biochem Biophys Res Commun* 2019, **519**(4):659–666.
7. Ding Y, Chen X, Liu C, Ge W, Wang Q, Hao X, Wang M, Chen Y, Zhang Q: **Identification of a small molecule as inducer of ferroptosis and apoptosis through ubiquitination of GPX4 in triple negative breast cancer cells**. *J Hematol Oncol* 2021, **14**(1):19.
8. Chen P, Li X, Zhang R, Liu S, Xiang Y, Zhang M, Chen X, Pan T, Yan L, Feng J *et al*: **Combinative treatment of beta-elemene and cetuximab is sensitive to KRAS mutant colorectal cancer cells by inducing ferroptosis and inhibiting epithelial-mesenchymal transformation**. *Theranostics* 2020, **10**(11):5107–5119.
9. Zhao L, Peng Y, He S, Li R, Wang Z, Huang J, Lei X, Li G, Ma Q: **Apatinib induced ferroptosis by lipid peroxidation in GC**. *GC* 2021, **24**(3):642-654.
10. Babjuk M, Burger M, Capoun O, Cohen D, Comperat EM, Dominguez Escrig JL, Gontero P, Liedberg F, Masson-Lecomte A, Mostafid AH *et al*: **European Association of Urology Guidelines on Non-muscle-invasive Bladder Cancer (Ta, T1, and Carcinoma in Situ)**. *Eur Urol* 2021.
11. Sylvester RJ, Rodriguez O, Hernandez V, Turturica D, Bauerova L, Bruins HM, Brundl J, van der Kwast TH, Brisuda A, Rubio-Briones J *et al*: **European Association of Urology (EAU) Prognostic Factor Risk Groups for Non-muscle-invasive Bladder Cancer (NMIBC) Incorporating the WHO 2004/2016 and WHO 1973 Classification Systems for Grade: An Update from the EAU NMIBC Guidelines Panel**. *Eur Urol* 2021, **79**(4):480–488.
12. Dashti A, Ebrahimi M, Hadjati J, Memarnejadian A, Moazzeni SM: **Dendritic cell based immunotherapy using tumor stem cells mediates potent antitumor immune responses**. *Cancer Lett* 2016, **374**(1):175–185.
13. Kono K, Nakajima S, Mimura K: **Current status of immune checkpoint inhibitors for GC**. *GC* 2020, **23**(4):565–578.
14. Schneider AK, Chevalier MF, Derre L: **The multifaceted immune regulation of bladder cancer**. *Nat Rev Urol* 2019, **16**(10):613–630.
15. Xue Y, Tong L, LiuAnwei Liu F, Liu A, Zeng S, Xiong Q, Yang Z, He X, Sun Y, Xu C: **Tumorinfiltrating M2 macrophages driven by specific genomic alterations are associated with prognosis in bladder cancer**. *Oncol Rep* 2019, **42**(2):581–594.
16. Lee DA: **Cellular therapy: Adoptive immunotherapy with expanded natural killer cells**. *Immunol Rev* 2019, **290**(1):85–99.
17. Fernandes JV, Cobucci RN, Jatoba CA, Fernandes TA, de Azevedo JW, de Araujo JM: **The role of the mediators of inflammation in cancer development**. *Pathol Oncol Res* 2015, **21**(3):527–534.

18. Johnston MP, Khakoo SI: **Immunotherapy for hepatocellular carcinoma: Current and future**. *World J Gastroenterol* 2019, **25**(24):2977–2989.
19. Zhou N, Bao J: **FerrDb**: **a manually curated resource for regulators and markers of ferroptosis and ferroptosis-disease associations**. *Database (Oxford)* 2020, **2020**.
20. Yoshihara K, Shahmoradgoli M, Martinez E, Vegesna R, Kim H, Torres-Garcia W, Trevino V, Shen H, Laird PW, Levine DA *et al*: **Inferring tumour purity and stromal and immune cell admixture from expression data**. *Nat Commun* 2013, **4**:2612.
21. Li T, Fan J, Wang B, Traugh N, Chen Q, Liu JS, Li B, Liu XS: **TIMER: A Web Server for Comprehensive Analysis of Tumor-Infiltrating Immune Cells**. *Cancer Res* 2017, **77**(21):e108-e110.
22. Newman AM, Liu CL, Green MR, Gentles AJ, Feng W, Xu Y, Hoang CD, Diehn M, Alizadeh AA: **Robust enumeration of cell subsets from tissue expression profiles**. *Nat Methods* 2015, **12**(5):453–457.
23. Rooney MS, Shukla SA, Wu CJ, Getz G, Hacohen N: **Molecular and Genetic Properties of Tumors Associated with Local Immune Cytolytic Activity**. *Cell* 2015, **160**(1-2):48–61.
24. Shi X, Huang T, Wang J, Liang Y, Gu C, Xu Y, Sun J, Lu Y, Sun K, Chen S *et al*: **Next-generation sequencing identifies novel genes with rare variants in total anomalous pulmonary venous connection**. *EBioMedicine* 2018, **38**:217-227.
25. Zhou Y, Zhou B, Pache L, Chang M, Khodabakhshi AH, Tanaseichuk O, Benner C, Chanda SK: **Metascape provides a biologist-oriented resource for the analysis of systems-level datasets**. *Nat Commun* 2019, **10**(1):1523.
26. Lv Z, Pang C, Wang J, Xia H, Liu J, Yan Q, Liu S, Liu M, Wang J: **Identification of a prognostic signature based on immune-related genes in bladder cancer**. *Genomics* 2021, **113**(3):1203–1218.
27. Chen DS, Mellman I: **Elements of cancer immunity and the cancer-immune set point**. *Nature* 2017, **541**(7637):321–330.
28. Qin X, Zhang J, Wang B, Xu G, Yang X, Zou Z, Yu C: **Ferritinophagy is involved in the zinc oxide nanoparticles-induced ferroptosis of vascular endothelial cells**. *Autophagy* 2021:1–20.
29. Zhang Z, Guo M, Li Y, Shen M, Kong D, Shao J, Ding H, Tan S, Chen A, Zhang F *et al*: **RNA-binding protein ZFP36/TTP protects against ferroptosis by regulating autophagy signaling pathway in hepatic stellate cells**. *Autophagy* 2020, **16**(8):1482–1505.
30. Hu XF, Yao J, Gao SG, Wang XS, Peng XQ, Yang YT, Feng XS: **Nrf2 overexpression predicts prognosis and 5-FU resistance in GC**. *Asian Pac J Cancer Prev* 2013, **14**(9):5231–5235.
31. Kawasaki Y, Ishigami S, Arigami T, Uenosono Y, Yanagita S, Uchikado Y, Kita Y, Nishizono Y, Okumura H, Nakajo A *et al*: **Clinicopathological significance of nuclear factor (erythroid-2)-related factor 2 (Nrf2) expression in GC**. *BMC Cancer* 2015, **15**:5.
32. Wei JL, Wu SY, Yang YS, Xiao Y, Jin X, Xu XE, Hu X, Li DQ, Jiang YZ, Shao ZM: **GCH1 induces immunosuppression through metabolic reprogramming and IDO1 upregulation in triple-negative breast cancer**. *J Immunother Cancer* 2021, **9**(7).

33. Pickert G, Myrczek T, Ruckert S, Weigert A, Haussler A, Ferreiros N, Brune B, Lotsch J, Tegeder I: **Inhibition of GTP cyclohydrolase reduces cancer pain in mice and enhances analgesic effects of morphine**. *J Mol Med (Berl)* 2012, **90**(12):1473–1486.
34. Hervouet E, Claude-Taupin A, Gauthier T, Perez V, Fraichard A, Adami P, Despouy G, Monnien F, Algros MP, Jouvenot M *et al*: **The autophagy GABARAPL1 gene is epigenetically regulated in breast cancer signatures**. *BMC Cancer* 2015, **15**:729.
35. Jacquet M, Guittaut M, Fraichard A, Despouy G: **The functions of Atg8-family proteins in autophagy and cancer: linked or unrelated?** *Autophagy* 2021, **17**(3):599–611.
36. Chen MS, Wang SF, Hsu CY, Yin PH, Yeh TS, Lee HC, Tseng LM: **CHAC1 degradation of glutathione enhances cystine-starvation-induced necroptosis and ferroptosis in human triple negative breast cancer cells via the GCN2-eIF2alpha-ATF4 pathway**. *Oncotarget* 2017, **8**(70):114588–114602.
37. Chen PH, Shen WL, Shih CM, Ho KH, Cheng CH, Lin CW, Lee CC, Liu AJ, Chen KC: **The CHAC1-inhibited Notch3 pathway is involved in temozolomide-induced glioma cytotoxicity**. *Neuropharmacology* 2017, **116**:300–314.
38. Jahn B, Arvandi M, Rochau U, Fiegl H, Goebel G, Marth C, Siebert U: **Development of a novel prognostic score for breast cancer patients using mRNA expression of CHAC1**. *J Comp Eff Res* 2017, **6**(7):563-574.
39. Yu FX, Johnston PA, Sudhof TC, Yin HL: **gCap39, a calcium ion- and polyphosphoinositide-regulated actin capping protein**. *Science* 1990, **250**(4986):1413–1415.
40. Pellieux C, Desgeorges A, Pigeon CH, Chambaz C, Yin H, Hayoz D, Silacci P: **Cap G, a gelsolin family protein modulating protective effects of unidirectional shear stress**. *J Biol Chem* 2003, **278**(31):29136–29144.
41. Kanai Y, Hediger MA: **The glutamate/neutral amino acid transporter family SLC1: molecular, physiological and pharmacological aspects**. *Pflugers Arch* 2004, **447**(5):469–479.
42. Dixon SJ, Patel DN, Welsch M, Skouta R, Lee ED, Hayano M, Thomas AG, Gleason CE, Tatonetti NP, Slusher BS *et al*: **Pharmacological inhibition of cystine-glutamate exchange induces endoplasmic reticulum stress and ferroptosis**. *Elife* 2014, **3**:e02523.
43. Cao Y, Dave KB, Doan TP, Prescott SM: **Fatty acid CoA ligase 4 is up-regulated in colon adenocarcinoma**. *Cancer Res* 2001, **61**(23):8429–8434.
44. Monaco ME, Creighton CJ, Lee P, Zou X, Topham MK, Stafforini DM: **Expression of Long-chain Fatty Acyl-CoA Synthetase 4 in Breast and Prostate Cancers Is Associated with Sex Steroid Hormone Receptor Negativity**. *Transl Oncol* 2010, **3**(2):91–98.
45. Ye X, Zhang Y, Wang X, Li Y, Gao Y: **Tumor-suppressive functions of long-chain acyl-CoA synthetase 4 in GC**. *IUBMB Life* 2016, **68**(4):320–327.
46. Sung YK, Hwang SY, Park MK, Bae HI, Kim WH, Kim JC, Kim M: **Fatty acid-CoA ligase 4 is overexpressed in human hepatocellular carcinoma**. *Cancer Sci* 2003, **94**(5):421–424.
47. Gonzalez-Sanchez L, Cobos-Fernandez MA, Lopez-Nieva P, Villa-Morales M, Stamatakis K, Cuezva JM, Marin-Rubio JL, Vazquez-Dominguez I, Gonzalez-Vasconcellos I, Salido E *et al*: **Exploiting the**

passenger ACO1-deficiency arising from 9p21 deletions to kill T-cell lymphoblastic neoplasia cells. *Carcinogenesis* 2020, **41**(8):1113–1122.

48. Guo S, Chen X: **The human Nox4: gene, structure, physiological function and pathological significance**. *J Drug Target* 2015, **23**(10):888–896.
49. Lu JP, Monardo L, Bryskin I, Hou ZF, Trachtenberg J, Wilson BC, Pinthus JH: **Androgens induce oxidative stress and radiation resistance in prostate cancer cells though NADPH oxidase**. *Prostate Cancer Prostatic Dis* 2010, **13**(1):39–46.
50. Yang WH, Ding CC, Sun T, Rupprecht G, Lin CC, Hsu D, Chi JT: **The Hippo Pathway Effector TAZ Regulates Ferroptosis in Renal Cell Carcinoma**. *Cell Rep* 2019, **28**(10):2501-2508 e2504.
51. Poursaitidis I, Wang X, Crighton T, Labuschagne C, Mason D, Cramer SL, Triplett K, Roy R, Pardo OE, Seckl MJ *et al*: **Oncogene-Selective Sensitivity to Synchronous Cell Death following Modulation of the Amino Acid Nutrient Cystine**. *Cell Rep* 2017, **18**(11):2547–2556.
52. Chen X, Zhu L, Ma Z, Sun G, Luo X, Li M, Zhai S, Li P, Wang X: **Oncogenic miR-9 is a target of erlotinib in NSCLCs**. *Sci Rep* 2015, **5**:17031.
53. Sondermann A, Andreghetto FM, Moulatlet AC, da Silva Victor E, de Castro MG, Nunes FD, Brandao LG, Severino P: **MiR-9 and miR-21 as prognostic biomarkers for recurrence in papillary thyroid cancer**. *Clin Exp Metastasis* 2015, **32**(6):521–530.
54. Saxena A, Shukla SK, Prasad KN, Ghoshal UC: **Analysis of p53, K-ras gene mutation & Helicobacter pylori infection in patients with GC & peptic ulcer disease at a tertiary care hospital in north India**. *Indian J Med Res* 2012, **136**(4):664–670.
55. Solcia E, Klersy C, Mastracci L, Alberizzi P, Candusso ME, Diegoli M, Tava F, Riboni R, Manca R, Luinetti O: **A combined histologic and molecular approach identifies three groups of GC with different prognosis**. *Virchows Arch* 2009, **455**(3):197–211.
56. Zepp JA, Zhao J, Liu C, Bulek K, Wu L, Chen X, Hao Y, Wang Z, Wang X, Ouyang W *et al*: **IL-17A-Induced PLET1 Expression Contributes to Tissue Repair and Colon Tumorigenesis**. *J Immunol* 2017, **199**(11):3849–3857.
57. Jin C, Lagoudas GK, Zhao C, Bullman S, Bhutkar A, Hu B, Ameh S, Sandel D, Liang XS, Mazzilli S *et al*: **Commensal Microbiota Promote Lung Cancer Development via gammadelta T Cells**. *Cell* 2019, **176**(5):998-1013 e1016.
58. Wu X, Yang T, Liu X, Guo JN, Xie T, Ding Y, Lin M, Yang H: **IL-17 promotes tumor angiogenesis through Stat3 pathway mediated upregulation of VEGF in GC**. *Tumour Biol* 2016, **37**(4):5493–5501.
59. Du F, Sun L, Chu Y, Li T, Lei C, Wang X, Jiang M, Min Y, Lu Y, Zhao X *et al*: **DDIT4 promotes GC proliferation and tumorigenesis through the p53 and MAPK pathways**. *Cancer Commun (Lond)* 2018, **38**(1):45.
60. Wu S, Chen M, Huang J, Zhang F, Lv Z, Jia Y, Cui YZ, Sun LZ, Wang Y, Tang Y *et al*: **ORAI2 Promotes GC Tumorigenicity and Metastasis through PI3K/Akt Signaling and MAPK-Dependent Focal Adhesion Disassembly**. *Cancer Res* 2021, **81**(4):986–1000.

61. Zhang Q, Wang X, Cao S, Sun Y, He X, Jiang B, Yu Y, Duan J, Qiu F, Kang N: **Berberine represses human GC cell growth in vitro and in vivo by inducing cytostatic autophagy via inhibition of MAPK/mTOR/p70S6K and Akt signaling pathways**. *Biomed Pharmacother* 2020, **128**:110245.

Figures

Figure 1

The protocol of our study procedures

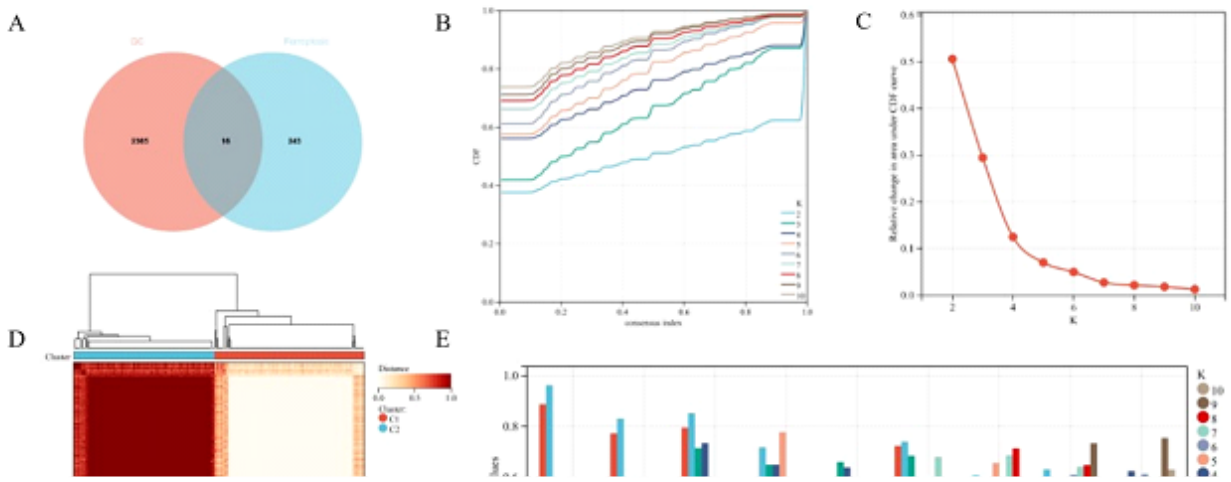

Figure 2

Molecular subtype identification based on ferroptosis

(A) Venn diagram, a prognostic gene for GC associated with ferroptosis. (B-E) Consistent clustering for GC patients. (F) Heat map of ferroptosis gene expression in two different subgroups. (G) Kaplan-Meier survival curves for two different subgroups.

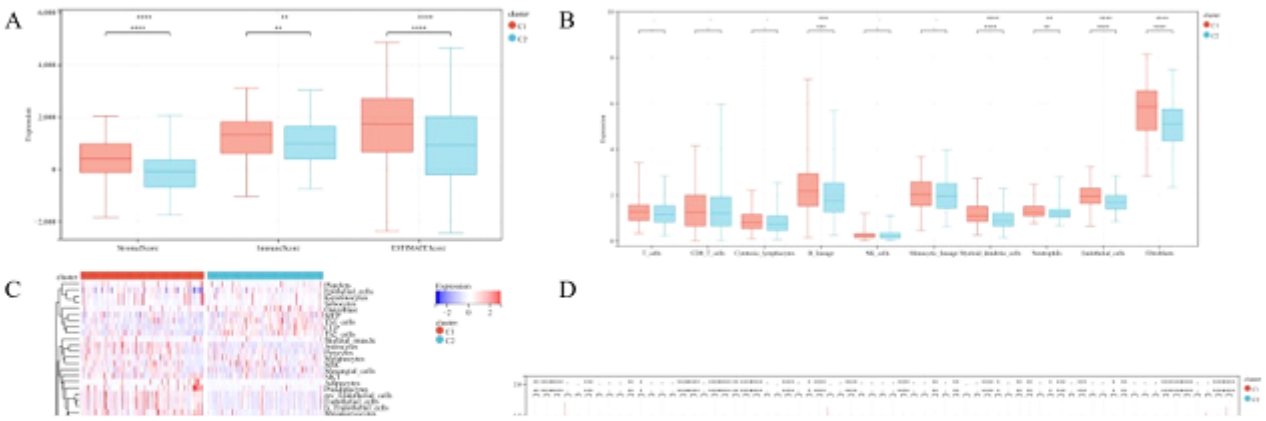

Figure 3

Immune microenvironment of two different molecular subtypes

(A) The ESTIMATE algorithm calculated the ESTIMATE score, immune cell infiltration degree and matrix score. (B) The MCPcounter algorithm was used to evaluate the immune cell infiltration level. (C-D) TIMER to assess immune cell abundance. The (E-F) CIBERSORT algorithm was used to calculate the level of tumor-infiltrating immune cells. *p < 0.05; **p < 0.01; ***p < 0.001.

Figure 4

Construction of risk signature based on prognosis genes related to ferroptosis and analysis of its relationship with immune infiltration status

(A) LASSO analysis with minimal lambda. (B)Distribution of survival status，risk score，and heat map of GC patients in the high and low-risk groups.(C) Survival curve of the GC patients in the two groups. (D) Forest map of multi-factor survival analysis. (E) Time-dependent ROC curve of the risk signature. (F) Stomal score, immune score, and ESTIMATE score in the high and low-risk groups. (G) Correlation between the key FRGs and the infiltration level of immune cells. *p < 0.05; **p < 0.01; ***p < 0.001.

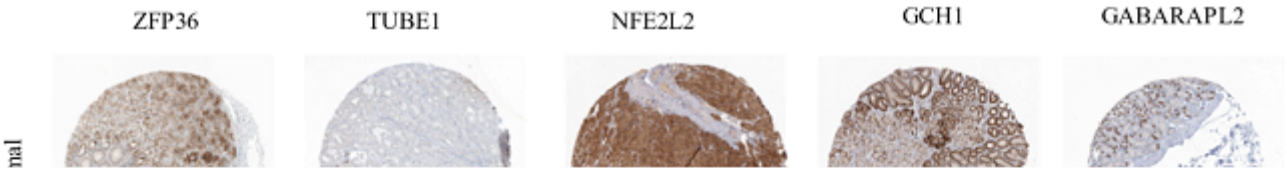

Figure 5

Immunohistochemical staining of key prognostic genes of ferroptosis

The expression of ZFP36, TUBE1, NFE2L2, GCH1, GABARAPL2, CHAC1, CAPG, ACSL4, and ACO1 in the HPA.

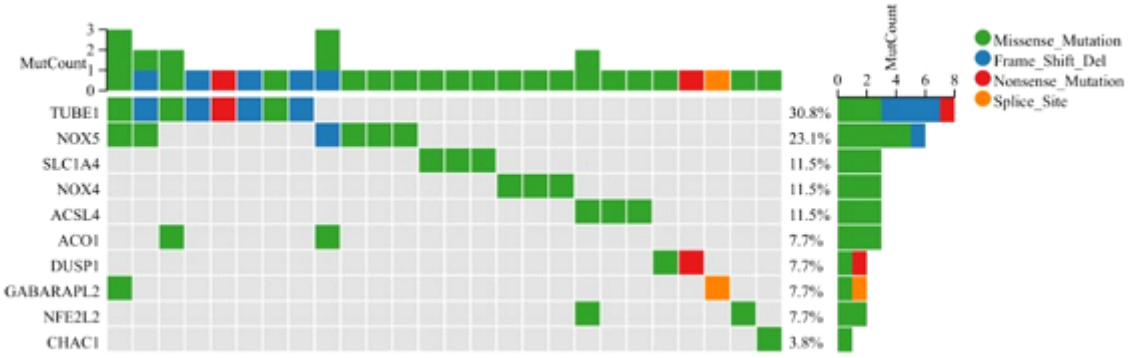

Figure 6

Somatic mutation number of key prognostic genes of ferroptosis

Figure 7

Validation of prognostic risk signature

Differences in risk scores among(A)Age, (B)Gender, (C)T, (D)N, (E) Stage, and (F)Grade. Survival curve of GC patients regrouped according to age (G-H), and gender (I-J). *p < 0.05; **p < 0.01; ***p < 0.001.

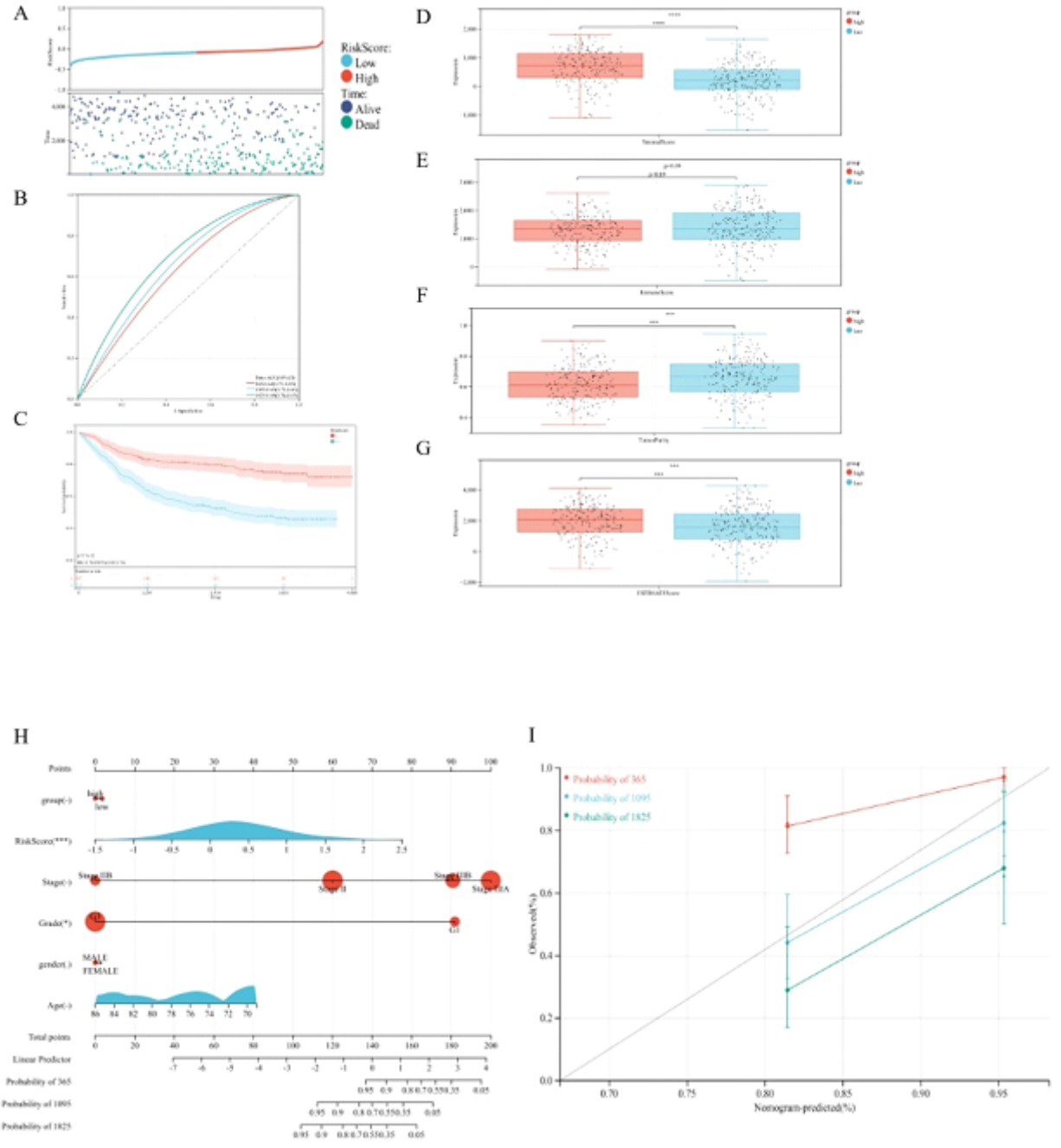

Figure 8

Validation of prognostic risk signature in validation cohort and the construction of Nomogram

(A) Distribution of survival status and risk score. (B) ROC curve of the risk signature in the verification cohort. (C) Survival curve of the patients in the high and low-risk groups in the validation cohort. (D–G) Stromal score, immune score, tumor purity, and ESTIMATE score calculated by ESTIMATE algorithm. (H) Nomogram integrating risk score and clinical features. (I) Calibration of the nomogram at 1,3, and 5 years in the TCGA. *p < 0.05; **p < 0.01; ***p < 0.001.

Figure 9

Identification of DEGs and functional enrichment analysis

(A)The volcanic map of DEGs. (B)The heat map of DEGs. (C-F) The BP, CC, MF, and the whole GO of DEGs. (G)The PPI analysis of GO enrichment analysis. (H)The enrichment circle diagram of KEGG enrichment analysis. (I)The PPI analysis of KEGG enrichment analysis. (J)The heat map of GSEA analysis results.

Supplementary Files

This is a list of supplementary files associated with this preprint. Click to download.

- rawdata.zip
- smallexp.xlsx
- GSEA.xlsx
- GEOe.xlsx
- GEOc.xlsx
- TCGAe.xlsx
- TCGAc.xlsx
- immunenormalize.xlsx
- DEG.xlsx
- vennData.csv
- COX.xlsx